IS-T-696

OPTICAL PROPERTIES OF Nb-Mo AND OTHER ALLOYS OF Nb WITH ITS NEAREST NEIGHBORS IN THE PERIODIC TABLE

Elizabeth Seyfarth Black

M. S. Thesis Submitted to Iowa State University

Ames Laboratory, ERDA
Iowa State University
Ames, Iowa 50011

Date Transmitted: October 1975

PREPARED FOR THE U. S. ENERGY RESEARCH AND DEVELOPMENT ADMINISTRATION UNDER CONTRACT NO. W-7405-eng-82

DISCLAIMER

Available from: National Technical Information Service
U. S. Department of Commerce
P.O. Box 1553
Springfield, VA 22161

Price: Microfiche $2.25

IS-T-696

Optical properties of Nb-Mo and other alloys of Nb with its nearest neighbors in the periodic table

By

Elizabeth Seyfarth Black

A Thesis Submitted to the
Graduate Faculty in Partial Fulfillment of
The Requirements for the Degree of
MASTER OF SCIENCE

Major: Physics

Approved:

David W. Lynch
In Charge of Major Work

R G Barnes
For the Major Department

M J Miller
For the Graduate College

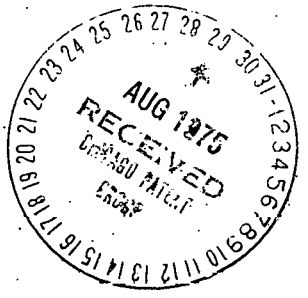

Iowa State University
Ames, Iowa
1975

TABLE OF CONTENTS

ABSTRACT

Optical properties of Nb alloys were investigated. Calorimetric measurements of absorptivity between 0.2 and 5.5 eV were taken for Nb samples with 20, 50, and 80% Mo and for Nb samples containing 10% Zr, 20% V, and 20% Ta. Reflectivity data for two of these samples in the ultraviolet region and known reflectivities for the pure metals to 35 eV provided the basis for extrapolation to high energies. The data were Kramers-Kronig analyzed to determine the dielectric function. The structure is discussed in terms of interband transitions as predicted by a rigid band model for the NbMo alloys.

THEORY AND TERMINOLOGY

Optical properties of solids have to do with the interaction of electromagnetic radiation with the particles - electrons and ions - in the material. Although studies of optical properties originally were concerned only with visible light, they have been extended to include a wider range of photon energy.

Maxwell's equations for the electric and magnetic fields in a solid can be written in microscopic form, in which the local variations in the fields are made explicit. For purposes of this paper, the macroscopic form of Maxwell's equations are more useful. Here the field vectors are an average over a large volume in the solid to avoid local field corrections. In Gaussian units one has (1):

$$\nabla \cdot \bar{B} = 0$$

$$\nabla \times \bar{E} = -\frac{1}{c}\, d\bar{B}/dt$$

$$\nabla \cdot \bar{D} = 4\pi \rho^{ext}$$

$$\nabla \times \bar{H} = \frac{1}{c}\, d\bar{D}/dt + \frac{4\pi}{c}\, \bar{J}^{cond} + \frac{4\pi}{c}\, \bar{J}^{ext}$$

$$\bar{D} = \bar{E} + 4\pi \bar{P}$$

$$\bar{H} = \bar{B} - 4\pi \bar{M}$$

The properties of the medium in which the light travels are described by the use of such quantities as the dielectric function, ϵ; the magnetic permeability, μ; and the optical conductivity, σ, where

$$\bar{D} = \epsilon\bar{E}$$

$$\bar{B} = \mu\bar{H}$$

$$\bar{J}^{cond} = \sigma\bar{E}$$

All these quantities are functions of the radiation frequency, ω. The dielectric function and conductivity are complex, and if anisotropic materials are to be included in the discussion, both quantities will be represented as complex tensors. As the frequency approaches zero, the real part of the optical conductivity becomes equal to the electric conductivity. If we combine these definitions with Maxwell's equations and assume no external charges, and therefore zero external current density, we obtain a set of equations which relate $\bar{E}$ and $\bar{H}$.

Several simplifications may be made when we solve these equations for a plane monochromatic light wave incident on a sample surface, this special choice being made because it corresponds to our experimental arrangement. As the wave approaches the surface, it travels in a vacuum where $\epsilon = \mu = 1$. The alloys under investigation have body centered cubic crystal structure. With respect to a coordinate system with three equivalent axes, the dielectric function may be expressed as a scalar rather than a tensor quantity (2). For the optical frequency range we take $\mu = 1$ in the solid as well as the vacuum. The experiment can be arranged with s- or p-

polarized light incident on the sample surface at a known angle φ.

The boundary conditions at the surface are that the tangential components of $\bar{E}$ and $\bar{H}$ and the normal components of $\bar{D}$ and $\bar{B}$ be the same on either side.

Let r be the ratio of the amplitudes of the reflected and incident waves, and θ be the phase difference between the two waves. The reflectivity, R, is just r^2, since R is the ratio of the intensities of reflected and incident radiation. A direct measurement of R and θ at a given frequency, ω, provides sufficient information for calculation of the dielectric function at that frequency. It may also be deduced from measurements of R taken at two different angles of incidence, or measurements of R for light of different polarizations. With thin films, one can measure both reflectivity and transmission.

When R and θ are measured independently of one another, it is not clear that the two quantities are related. But with an argument based on causality it can be shown that (1):

$$\theta(\omega) = \frac{1}{2\pi} \int_0^\infty \frac{d \ln R(\omega')}{d\omega'} \ln\left[\frac{\omega - \omega'}{\omega + \omega'}\right] d\omega'$$

This means that if we know R for all frequencies, we can compute the phase shifts. In practice, R is measured over some finite range and values are extrapolated outside that range to use in a numerical calculation of θ. Integral relations between two functions of frequencies, such as this

one between θ and R, have been given the name Kramers-Kronig relations.

With both R and θ known, the dielectric function may be calculated as follows:

For s-polarized light,

$$\epsilon(\omega) = Z^2(\omega)\cos^2\varphi + \sin^2\varphi$$

For p-polarized light,

$$\epsilon(\omega) = \frac{Z^2(\omega)}{Z(\omega)\cos^2\varphi}\left[\,1 \pm \left(1 - \frac{4\cos^2\varphi\sin^2\varphi}{Z^2(\omega)}\right)^{\frac{1}{2}}\,\right]$$

where

$$Z(\omega) = \frac{1 + r(\omega)\exp(i\theta(\omega))}{1 + r(\omega)\exp(i\theta(\omega))}$$

In the equation for p-polarized light, the sign ambiguity is resolved by choosing the solution giving a positive value for the imaginary part of the dielectric function (3).

Once has been determined, other quantities may be calculated which may be more useful for certain purposes. The real and imaginary parts of the complex quantities are defined so that $\epsilon = \epsilon_1 + \epsilon_2$ and $\sigma = \sigma_1 - \sigma_2$. We also have $\epsilon = (n + ik)^2$ where n is the refractive index and k is the extinction coefficient which describes the damping of the wave as it travels in an absorbing medium. σ, n, and k are given by

$$\sigma_1 = \frac{\omega}{4\pi}\,\epsilon_2 \qquad \sigma_2 = \frac{\omega}{4\pi}\,(\epsilon_1 - 1)$$

$$n = \left[\tfrac{1}{2}\left(\sqrt{\epsilon_1^2 + \epsilon_2^2} + \epsilon_1\right)\right]^{\frac{1}{2}} \qquad k = \left[\tfrac{1}{2}\left(\sqrt{\epsilon_1^2 + \epsilon_2^2} - \epsilon_1\right)\right]^{\frac{1}{2}}$$

From similarity in the spectra of many metals and the theory of electron band structure in solids, it is possible to develop some notion of the expected behavior of the transition metal alloys being studied. For a complete appreciation of the theory one must take a quantum mechanical viewpoint. Each electron exists in a state with a well-defined energy. Absorption or emission of a quantum of energy occurs when the electron makes a transition to another state.

Such a transition represents either an intraband or interband contribution to the absorption, depending on whether the final and initial states are in the same energy band or different bands. For metals the conduction band consists of both occupied states below the fermi level and empty states above. Thus the conduction band electrons are the ones which will be making intraband transitions. A classical picture is useful in visualizing the intraband contribution to absorption. Although it has limitations, the resulting expression for $\epsilon(\omega)$ is the same as would be derived quantum mechanically.

The simplest model is that of Lorentz, in which the electrons are treated as classical oscillators. The time varying electric field exerts a force $-e\bar{E}_o \exp(-i\omega t)$ on the electrons. They are attracted back to their equilibrium site in the lattice by a restoring force $-m\omega_o^2 \bar{x}$. The oscillation

is damped by a force $m\gamma d\bar{x}/dt$. Solving the equation of motion gives

$$x = -\frac{e\bar{E}_o}{m} \quad \frac{\exp(-i\omega t)}{(\omega_o^2 - \omega^2) - i\gamma\omega}$$

The polarization $\bar{P} = -Ne\bar{x}$ where N is the number of electrons. The dielectric function is then

$$\epsilon = 1 + 4\pi\bar{P}/\bar{E} = 1 + \frac{4\pi Ne^2/m}{(\omega_o^2 - \omega^2) - i\gamma\omega}$$

The free-electron component is obtained from the Lorentz model with $\omega_o = 0$ since the conduction electrons are not tied down to any particular site. The mass m is replaced by an effective mass m* and γ may be written as $1/\tau$ where τ is the mean time between scattering events. These are the same scattering events which determine the electrical resistivity of the sample. With the plasma frequency ω_p defined so that $\omega_p^2 = 4\pi Ne^2/m^*$, one obtains the Drude expression:

$$\epsilon = 1 - \frac{\omega_p^2}{\omega^2 + i\omega/\tau}$$

When one has experimentally determined values for ϵ, the intraband term cannot easily be separated out from the total. However, at small frequencies, the photon energy is less than would be necessary for an electron to make a transition to one of the empty bands above the Fermi level. In this region, which for metals is in the infrared, the shape of the dielectric function will be as predicted by the Drude model.

To treat the more complicated shape of the curve at higher energies we will need to derive the quantum mechanical expression for the dielectric function including interband effects.

To begin, we may write down the Hamiltonian for a solid with N electrons per unit volume.

$$H = \frac{1}{2m} \sum_{j=1}^{N} [\bar{p}_j - \frac{e}{c} \bar{A}^{ext}(\bar{r}_j,t)]^2 + \sum_{j=1}^{N} V_j(\bar{r}_j)$$

$$+ \frac{1}{2} \sum_{i,j}{}' \frac{e^2}{|\bar{r}_i - \bar{r}_j|} + I + \sum_{i=1}^{N} e\,\varphi^{ext}(\bar{r}_i,t)$$

The momentum operator $\bar{p} = -i\hbar\nabla$. V is the periodic crystal potential seen by the electrons. The third summation gives the Coulomb energy between all pairs of electrons and I is the energy of the ion cores interacting with one another (1).

Band theorists who calculate the eigenstates of such a system use the Hamiltonian H_0, obtained from H by letting the external fields $\bar{A}$ and φ equal zero. The solutions will be Bloch functions having the periodicity of the lattice, $\psi_j(\bar{r}) = \exp(i\bar{k}_j \cdot \bar{r})\ u_j(\bar{k}_j,\bar{r})$ with energy E_j. Different approximation methods may be used, the choice depending on the system under consideration. A simplifying feature of all these techniques is that the nuclei are considered fixed in place. Attention is focused on the wavefunctions of a single electron. The effect of the other electrons is included in the field acting on the single electron (4). The wave

functions are expressed as expansions of some complete set of exact functions, in combinations which will give the symmetry required at different points in the unit cell. Various parameters can be adjusted to fit known properties of the material. For Nb and Mo, the energy bands have been calculated with the use of augmented plane waves (5,6).

To get at the optical properties we must include the effect of the radiation. As before, let the radiation have time dependence $\exp(-i\omega t)$. Including the spatial dependence gives $\bar{E} = E_o \hat{e} \exp(i\bar{k}_o \cdot \bar{r} - i\omega t)$. We choose the Coulomb gauge with $\varphi^{ext} = 0$ and $\bar{A}^{ext} = A_o \hat{a} \exp(i\bar{k}_o \cdot \bar{r} - i\omega t)$. This choice of gauge insures that $\bar{A}$ and $\bar{p}$ commute and provides a relationship between A_o and E_o. $\bar{E} = -(1/c)\, d\bar{A}/dt$ so that $E_o = i\omega A_o / c$.

The difference between H and H_o is taken as a perturbation term, H'. The term of order $\bar{A}^2$ is dropped and we have

$$H' = \frac{e}{mc} \bar{A} \cdot \bar{p}$$

$$= -\frac{e\hbar}{m\omega} E_o \exp(i\bar{k}_o \cdot \bar{r}) \; \hat{a} \cdot \nabla \; \exp(-i\omega t)$$

In this last expression for H', the time dependent term has been set apart from the rest.

Consider a transition from an initial state Ψ_i with energy E_i to a final state Ψ_f with energy E_f. These states are eigenstates of the unperturbed Hamiltonian. Time-dependent

perturbation theory gives the transition rate,

$$W_{if} = \frac{2\pi}{\hbar} \left| \int d\bar{r}\, \psi_f^{*} \left(-\frac{e\hbar}{m\omega} E_o\right) \exp(i\bar{k}_o \cdot \bar{r})\, \hat{a}.\nabla\psi_i \right|^2 \delta(E_f - E_i - \hbar\omega)$$

This is just the transition rate between two particular states. We assume that initially an electron is in state ψ_i while state ψ_f is empty. W_{if} should actually be weighted by $f(E_i/T)\,(1-f(E_f/T))$ which is the probability of the initial state being occupied and the final state being empty. f is the Fermi-Dirac distribution function (7). This factor will be omitted from here on, with the understanding that transitions are from full initial states to empty states.

Look at the squared term in W_{if}. The states are Bloch wavefunctions and integration will give zero unless $\bar{k}_f = \bar{k}_i + \bar{k}_o$. This is the conservation of momentum condition. Since the radiation wave vector $\bar{k}_o$ is much smaller than either $\bar{k}_f$ or $\bar{k}_i$, the only possible transitions will be vertical ones, that is, $\bar{k}_f \approx \bar{k}_i$. If we define $\bar{M}_{if} = \int d\bar{r}\, u_f^{*}(\bar{k},\bar{r})\, \nabla u_i(\bar{k},\bar{r})$ then the expression for W_{if} reduces to a more concise form,

$$W_{if} = \frac{2\pi}{\hbar} \left(\frac{e\hbar}{m\omega} E_o\right)^2 \left| \hat{a}.\bar{M}_{if} \right|^2 \delta(E_f - E_i - \hbar\omega)$$

Since it is impossible to identify transitions between two particular states, we need an expression for the total rate of transitions between any states involving the absorption of a photon of a particular energy. All transitions between a given band and a higher, empty band will be included if we multiply by the electron density of states, $1/4\pi^3$, and

integrate over $\bar{k}$-space. Then one sums the results for all pairs of bands between which transitions will occur. The total transition rate is

$$W_{tot} = \sum_{bands} \int \frac{d\bar{k}}{4\pi^3} W_{if}$$

The energy lost in these transitions is $\hbar\omega W_{tot}(\omega)$. It is also $\sigma_1(\omega)\ 2E_o^2$, so we can find the conductivity

$$\sigma_1(\omega) = \frac{\hbar\omega}{2E_o^2} W(\omega) = \frac{e^2\hbar^2}{4\pi^2 m^2 \omega} \int d\bar{k}\ |\hat{a}.\bar{M}_{if}|^2\ \delta(E_f - E_i - \hbar\omega)$$

and

$$\epsilon_2(\omega) = \frac{4\pi}{\omega}\sigma_1(\omega) = \frac{e^2\hbar^2}{\pi^2 m^2 \omega^2} \int d\bar{k}\ |\hat{a}.\bar{M}_{if}|^2\ \delta(E_f - E_i - \hbar\omega)$$

The matrix element $\bar{M}_{if}$ is not always easy to calculate, so sometimes one approximates without it. Assuming $|\hat{a}.\bar{M}_{if}|^2$ is a slowly varying function of $\bar{k}$, it can be pulled outside the integral. What is left is known as the joint density of states $J(\omega)$.

$$J(\omega) = \int \frac{d\bar{k}}{4\pi^3}\ \delta(E_f - E_i - \hbar\omega)$$

One expects that $\epsilon(\omega)$ will be roughly proportional to $J(\omega)$, the two curves having structure at the same values of ω, though not corresponding exactly in magnitude everywhere. Such an assumption was made by Pickett and Allen (8), who used the band calculations for Nb and Mo to obtain $J(\omega)$, which they then compared with experimental results for $\epsilon(\omega)$.

The joint density of states may be expressed as a surface integral instead of a volume integral.

$$J(\omega) = \frac{1}{4\pi^3} \int \frac{dS}{|\nabla_k(E_f - E_i)|}$$

The integration is performed over the surface in $\bar{k}$-space for which $E_f(\bar{k}) - E_i(\bar{k}) = \hbar\omega$. In this form it is clear that states for which the denominator equals zero will make a large contribution to the integral. Such points are called critical points and correspond to maxima, minima, or saddle points in $E_f - E_i$. Symmetry critical points are those at which $\nabla_k E_f = \nabla_k E_i = 0$. Their occurrence may be predicted solely on the basis of the symmetry requirements at particular values of $\bar{k}$. Some symmetry points commonly referred to are illustrated in figure 1. In semiconductors, features due to critical points have been identified in experimental curves of $\sigma(\omega)$ or $\epsilon(\omega)$. In metals, it has been found that critical point structure is there but does not show up clearly, perhaps because of a larger background of intraband transitions. Also, metals seem to have large volumes in $\bar{k}$-space for which the denominator is small, but not zero.

The general procedure as has been described is used for pure metals. To sum up briefly, one starts with a periodic lattice potential term in the Hamiltonian. Then the energy bands are calculated, and the location of the Fermi level is determined by the number of valence electrons. These electrons, of course, fill the lowest energy states in the bands. If light is absorbed in direct interband transitions,

time dependent perturbation theory gives an expression for the imaginary part of the dielectric function, which in the constant matrix approximation will be proportional to the joint density of states.

For the bcc transition metals Nb and Mo, this approach has been successful (9,10,11,12). With the direct transition model, peaks in the experimental ϵ_2 curve have been identified with transitions occurring at particular regions or points in $\bar{k}$-space. However, the optical data and calculations done thus far for such metals have not been able to rule out absorption by indirect transitions (12). For alloys, an impurity is probably involved in such a transition. Other mechanisms are also possible (13). If some of the momentum is carried away by impurity scattering, a phonon, or some other mechanism, we may no longer assume the transition is vertical.

The very fact of alloying means increased disorder. The arrangement of two types of nuclei make the crystal lattice non-periodic. Thus the wavevector may not even be a good quantum number under these conditions. But we would like to be able to describe the alloys in a methodical way, based on our understanding of the pure metals. To describe alloys, we must make some modifications in the methods used in treating the pure metals. At this point in time, alloy theory is under development and we have a choice of several different

approaches. Proposed models include the rigid band model (RBM), the virtual crystal model (VBM), the coherent potential approximation (CPA), and the virtual bound state (VBS) (14,15).

RBM was the first model suggested for alloys. According to it, one assumes the band structure of the pure metal persists unchanged when a second type of atom is introduced into the lattice. The electron concentration, though, changes if the two atoms have a different valence number, and this causes a corresponding change in Fermi level. Apart from this change in Fermi level, the treatment is the same as for the pure metal which is the solvent and whose energy bands are known. RBM predicts no change in the spectra for alloys of two metals with the same valence number. Two of the alloys we examine are of this type, NbTa and NbV. A limitation of the RBM is that it cannot in general be applied to alloys in which the concentrations of the two types of atoms are nearly equal. Some workers have improved the RBM by taking into account localized screening of the solute atoms (14).

The RBM has been applied to noble metals alloyed with small amounts of a polyvalent metal. The system of NbMo alloys is a good candidate for treatment according to the RBM, because the pure metals Nb and Mo have nearly identical energy bands. For any intermediate compositions, then, the

Fermi level would be in between the Fermi level for Nb and that for Mo. Imagine a transition between states just on either side of the Fermi level for some alloy composition. For some other composition, it may happen that these same two states are both below the Fermi level. A transition would not occur in the latter case, because the higher energy state is already occupied. We expect that what differences we see will be due to those states which are above the Fermi level for one alloy and below for another.

The VCM is similar to the RBM in that it is applicable to metals in which the electrons are non-localized. VCM, unlike RBM, allows for changes in the shape of the energy bands on alloying. The VCM uses as its starting point the periodic crystal potentials for the two metals. One then writes the potential for the alloy lattice as a linear combination of the two pure metal potentials. The coefficients in the linear combination are the concentration of the metal atoms occurring in the alloy. After writing this potential, one must use it in solving the Hamiltonian and computing the energy bands for the alloy. This linear relationship amounts to an assumption that the electron wave function is nearly equal in magnitude at both types of atoms. If an electron shows a preference for one atom type, as might be the case with a d-electron, then one atom type would be charged with respect to the other, and the VCM would not hold so well.

With either the VCM or CPA, any concentration of an alloy may be considered. CPA has proved to be especially useful in treating alloys with strong local potentials, such as transition metals. The CuNi alloy system has been thoroughly studied using a CPA approach (14). The CPA is based on multiple scattering theory for disordered systems. An electron undergoes scattering from the atoms of either type as it moves in the alloy. CPA finds exactly the scattering from one scatterer, replacing all the rest by an effective medium in which no scattering of electrons occurs. In the CPA one starts with the density of states for the two pure metals which are combined to form the alloy. Using these as a starting point, one then must arrive at a density of states for the alloy, which will in general not be a linear combination of the densities of states of the metals, but something more complicated.

The VBS model has been primarily used for noble metal-transition metal alloys. The transition metal impurity will have assiciated with it both s and d electron states; the noble metal itself has only s states. VBS theorizes that the density of states of the alloy will differ from that of the pure metal by the addition of a peak centered at the resonant energy level of the impurity d states. Optical absorption will be due to transitions from d to s states as well as transitions from one s state to another. VBS is limited to

low impurity concentrations for which the interaction of impurities with each other can be ignored. It may be applied to a host metal with a d-state provided that the energy of the d-electrons in the host metal does not come close or overlap with the energy of the virtual state. It is mentioned only for the sake of completeness, since it is not readily applicable to the transition metal alloys here under investigation.

It will be interesting to learn if there is an increase in indirect transitions in the alloys as compared to the pure metals (16). An increase in scattering by the non-periodic alloy lattice would cause more interactions in which an optically excited electron drops to a lower energy state, or another electron recombines with a hole. If the lifetime for such processes is short, then the uncertainty principle tells us that the energy absorbed in the transition to the excited state will not be exactly known. Such an increase in scattering and indirect transitions would show up as broadening of the absorption spectra of the alloys.

EXPERIMENTAL TECHNIQUES

The material from which the alloys were made was obtained within the Ames Laboratory, ERDA. The ingredients were measured out in the correct proportions by weight so as to give the desired final composition and then were electron beam melted. I used a spark cutter to cut slices of approximate dimensions .44" x .37" x .07" from each button, choosing sections which appeared relatively free of small holes or impurities. Rough polishing was done with water on #600 emery paper.

The worked surface was removed by electropolishing. All samples with 80 or 90 percent Nb were electropolished in a 2% sulfuric acid solution at about 200K. Nb and Ta will not electropolish in perchloric acid as will others of the transition metals. For the samples with 50 and 80 percent Mo, use of a 6% perchloric in methanol solution resulted in a satisfactory surface.

The final surfaces looked smooth and shiny to the eye. Grain boundaries, pits, and some impurities were visible when the samples were viewed under the microscope, but these accounted for only small fractions of the total surface area. The measured reflectivity will be determined largely by the area of surface of the alloy itself.

After the final polish and before they could be loaded into the calorimeter, the samples were exposed to air for

intervals varying from 10 to 30 minutes. During this time an oxide layer forms on the surface, but it will be thin because these metals oxidize slowly (17).

The calorimetric method with which the low energy data was obtained will be described briefly since a thorough report may be found elsewhere (18,19).

After passing through a double prism monochromator, the light beam is focused on a flat, polished sample surface with a near normal angle of incidence. An absorber is positioned so as to catch the portion of the beam reflected from the sample. The absorber is coated with gold black, a material which will absorb over 99 percent of the light it receives for all frequencies in our range of interest. Both sample and absorber heat up, the temperature changes depending on the amount of radiant energy absorbed. A steady state, constant temperature quickly results as the heat due to radiation is balanced by the same amount of heat lost by conduction through copper wires to the base of the flange which acts as thermal ground.

Small heat capacities are desirable to give appreciable changes in temperature even when the incident power is small. For this reason the calorimeter is maintained at a temperature near 4.2 K while in operation. It is immersed in a dewar of liquid helium, which in turn fits within an outer dewar containing liquid nitrogen.

Before cooling, the calorimeter is pumped out to a pressure of about 10^{-6} torr. An ion pump keeps the vacuum good, and once helium has been added, the pressure drops to 10^{-8} torr or less. This vacuum minimizes heat loss by conduction or by convection and prevents a rapid boil off of helium which would otherwise occur.

Carbon resistor thermometers whose resistivities vary rapidly with temperature near 4.2 K are mounted on copper blocks in back of the sample and absorber. The circuitry is arranged so that one measures the voltage across the thermometer resistor using a potentiometer. The voltage could be used to find the temperature, but this is not done since a comparison technique will allow the absorptivity of the sample to be determined.

Heater resistors, each 1000 ohms, are attached to the copper blocks behind the sample and absorber. One cuts off the light with a shutter and turns on and adjusts the heater current until the potentiometer reads the same voltage as before. The assumption is that a given amount of power will result in the same equilibrium temperature, whether applied as light or electrical power. The fine adjustments are made with the help of null detectors whose zero points are set to coincide with the thermometer voltage when light shines on the sample.

For a thick sample there is no transmission and the absorptivity, A, is equal to 1 - the reflectivity, R, We measure directly V_a and V_s, the voltages across standard resistors in parallel with the absorber and sample, respectively. (V_a/V_s) gives the ratio of the power at the absorber to that at the sample. Then, since A is the ratio of power at the sample to total incident power, we have

$$A = \frac{1}{1 + (V_s/V_a)^2}$$

The data are taken point by point, with the photon energy known from the drum number on the monochromator. It has been calibrated using as references atomic emission and atmospheric absorption lines, interference filters, and, in the infrared region, a polystyrene film with known transmission. With the appropriate combination of the globar, tungsten filament bulb, or mercury arc lamp, and quartz or calcium fluoride prisms, slit width can be adjusted to give sufficient incident power for photon energies from 0.2 to 4.5 or more eV.

An alternative method which has been often used in determining reflectivity is one in which the intensities of the incident and reflected beams are directly measured. For highly reflecting metals, a small uncertainty in these measured intensities gives a much larger error in the calculated reflectivity, and for these samples the calorimetric technique has a definite advantage. Above 5 eV there is no

good high intensity light source to be used with the calorimeter. Furthermore, prisms which are transparent for visible light have lower transmission for ultraviolet radiation. Since the reflectivity of metals is typically much lower at high frequencies than in the infrared and visible range, calorimetry has no special advantage for the ultraviolet.

The vacuum ultraviolet measurements were taken by C. G. Olson using synchroton radiation from the electron storage ring facility located at Stoughton, Wisconsin (20,21). Several differences may be noted. A grating monochromator is used, and the light incident on the sample is polarized. The sample is mounted within the vacuum system at room temperature. Data may be obtained with this equipment between 2 and 36 eV of photon energy. The curve in the overlap region is drawn so as to give a smooth fit between the calorimeter data and the data from Stoughton.

ANALYSIS AND DISCUSSION OF RESULTS

The data obtained with the calorimeter are displayed in figures 2 and 3. What is shown is a smoothed curve drawn through the experimental points. Scatter among data points occurred mostly at the limits, for photon energy greater than 4.0 eV or less than 0.3 eV. The most that the data points typically differed from the smoothed curve was by 0.02 in absolute value for absorptivity. Some curves do not extend as far because fewer measurements were completed.

Figure 2 shows the measured absorptivity for three NbMo alloys, and for comparison, the previously measured absorptivity for Nb and Mo. The four elements most closely adjacent to Nb in the periodic table are Zr and Mo (same row) and V and Ta (same column). Figure 3 shows the absorptivity of four Nb alloy samples, each containing 10 or 20 percent of one of these elements. The absorptivity of Nb itself is included for easy reference. Note that the curves for the alloys are comparable in magnitude to those for the pure metals and show definite structure. This alone suggests that the alloys do have well-defined energy bands in spite of the disorder introduced by the presence of two types of atoms. We would expect the structure to show broadening and flattening of peaks if there was a large increase in the number of indirect transitions as compared to the pure metals. The NbV curve is more smeared out than the others, so indirect

transitions could play a part in the behavior of this alloy. For the rest of them, we proceed with the assumption that $\bar{k}$ is a good quantum number and that all transitions are direct.

To better compare with the theoretical predictions from the density of states we need to perform the Kramers-Kronig analysis for the phase shift and then calculate the dielectric function or the optical conductivity. The shape of the imaginary dielectric function is dominated by a large negative slope due to a background of intraband absorption. Multiplying by a factor of photon energy makes the features of the curve stand out more clearly from the background. The conductivity is proportional to this product of photon energy times imaginary dielectric function, so we chose to show the conductivity.

The Kramers-Kronig integral is evaluated numerically with a trapezoidal approximation. Our computer program is based on one developed by Kreiger, Olechna, and Story (22). For the analysis we took 10 degrees as the angle of incidence and assumed p-polarization. For small angles, the result is rather insensitive to the angle used. The light used in the calorimetric work is of undetermined polarization, but the high energy extrapolations were based on data from the storage ring which were taken using p-polarized light.

Lock at figure 4. Here are the reflectivity results for Nb(80)Mo(20) sample to 30 eV. The data from the calorimeter

and from Stoughton have been smoothly joined at about 4.1 eV. The dashed line gives the high energy data for pure Nb. The lower part of the figure shows the calculated conductivity. The solid curve uses the data from the sample out to 36 eV. The dashed curve shows the effect of using the pure Nb reflectivity data above 4.1 eV in lieu of that of the sample. Such an extrapolation was necessary for the other alloys for which high energy data were not yet available. So we would like to estimate how much error is introduced by the procedure.

The errors introduced by extrapolations in the unknown region of the spectra can be more thoroughly investigated using an exact expression for a model system giving both reflectivity and conductivity. The reflectivity is then used, with or without made-up extrapolations as the data from which the conductivity may be calculated numerically (23).

Although the dashed conductivity curve in figure 4 has extra bumps at higher energies, it is encouraging to observe that at low energies - less than 5.0 eV - the two curves have peaks appearing at nearly identical values of photon energy. There is some change in magnitude, however. We will thus be able to draw conclusions about the energy of photons absorbed in interband transitions, although we will be cautious about comparing the relative importance of such transitions.

The conductivity plotted as a function of photon energy is shown in figures 5 and 6. For all the predominantly Nb alloys in figure 6, the high energy extrapolation used in calculating the conductivity was that of pure Nb. In each case the calorimeter data was used to as high a value of photon energy as possible.

In figure 5, the curves for Nb(100), Mo(100), and Nb(80)Mo(20) used data from Stoughton to extend the calorimeter data to higher energy for use in the numerical calculation of the conductivity. For the Nb(50)Mo(50) sample, the reflectivity used for any given frequency in the ultraviolet was an average of the reflectivity for Nb and Mo for that frequency. The data for the Nb(20)Mo(80) sample was extrapolated to higher energies using the data for Mo(100).

The graphs of conductivity will now be discussed with reference to the energy bands. This gives a way to relate absorption of a particular photon energy to the points at $\bar{k}$-space at which transitions involving this photon occur.

The energy bands in figure 8 are for Nb; those for Mo are comparable, with the Fermi level shifted up about 0.12 Ry. A relativistic calculation would look nearly the same except that in places where the bands cross, relativistic considerations remove the degeneracy. The bands approach each other, then bend away without actually crossing. An example of such a crossing is the one between the second and

third lowest energy bands near G. There will be spin orbit splitting for some of the relativistic bands and a breakdown of the selection rules. The spin orbit effects are too small to show up in these metals.

Starting at low energies, we have interband transitions beginning to occur at 0.9 eV in photon energy for Nb. Interband transitions show up at lower energies as the Mo concentration increases - 0.85 eV for 50% Mo, 0.7 eV for 80% Mo, and 0.6 eV for pure Mo. For the Nb(80)Ta(20) sample, interband transitions seem to start at 0.8 eV. The onset of interband transitions occurs somewhat higher in energy for the NbV and NbZr alloys - at 0.95 and 1.1 eV respectively. It is difficult to assign these low energy transitions to any particular region in $\bar{k}$-space.

Between 1.0 and 2.0 eV, curves for the samples with 50% or more Nb increase linearly with no outstanding features. For the 80% Mo sample there is a broad shoulder centered around 1.3 eV. In the pure Mo spectra this same feature shows up as a more abrupt shoulder at 1.8 eV. Most likely this corresponds to transitions from band 3 at the Fermi level to band 4 near Δ in the Brillouin zone (12).

Next there is a relatively strong peak near 2.4 eV which shows up in all the samples. This absorption has been identified as being due to transitions from the third band at Σ to the next higher band running parallel with the same Σ_1

symmetry (8,10). This peak seems strongest in the alloys with more Mo, which has an additional valence electron. The lower band is only partly filled in Nb. The Fermi level will increase with greater Mo concentration, thus giving more filled states in the lower band, and a greater probability of transitions occurring. Such an effect could explain the shift in sharpness of the 2.4 eV peak. Absorption at 2.4 eV might also be brought about in Mo by transitions from states at the Fermi level in band 4 near Δ to band 5.

Additional peaks occur near 4.2 eV, and for Nb, at 5.2 eV. The position of the one peak shifts from 4.4 for the Nb rich alloys to 4.2 for those composed mostly of Mo. Transitions accounting for the 4.3 eV peak are thought to include ones from band 2 to 4 at N, and those from band 1 to 4 along the G direction and near Δ (10). Transitions from band 3 to band 5, near Δ which involve an absorption of slightly less energy, 4.0 eV, will be important only in the Mo rich alloy (12). Pickett and Allen also find that some of the absorption at this energy is due to transitions at $\bar{k}$ = (1/2, 1/4, 1/4) (8). The additional peak in Nb at 5.2 eV has been identified with transitions from band 2 to band 5 near N.

Above 5.0 eV it becomes progressively more difficult to make assignments of particular bands in $\bar{k}$-space which give rise to absorption at particular energies.

Our only basis for choosing among the different theories which have been proposed for dealing with alloys is to see how well our experimental results can be understood in terms of the theories.

We begin with the rigid band model (RBM). Theoretical predictions of the conductivity for a series of NbMo alloys are shown for comparison in figure 7. The curves are based on the joint density of states calculated by Pickett and Allen in the rigid band approximation. What is shown represents only the interband contribution to conductivity. Above 3 eV, the density of states, and thus the conductivity will be essentially the same for Nb and Mo. The peak at 2.4 eV for all compositions is in excellent agreement with the experimental data.

Theory predicts humps at 1.55 and 1.8 eV for Nb, and again at 1.8 eV for an 80% Nb 20% Mo composition. There is a suggestion of a weak hump in the 20% Mo data at 1.7 eV, but nothing at all in the Nb data in this region. However, even moderate changes in the matrix elements would account for a peak not appearing in the conductivity curve which does appear in the joint density of states. A broad shoulder appears near 1.6 eV in the curve calculated for an 80% Mo composition. In the curve calculated for pure Mo, the shoulder becomes more abrupt and occurs at 2.1 eV. Here there is good qualitative agreement with the shape of the ex-

perimental curve, but the predicted position of the shoulders is .3 eV higher than the actual positions.

The other models for alloys - the coherent potential approximation(CPA), or the virtual crystal model(VCM) - are more difficult to compare with the data. What is really needed to evaluate the usefulness of these theories as applied to the bcc transition metals is some theoretical calculations to compare with experiment. The CPA might well give good agreement, with the exception of NbZr, since the density of states for Zr would be that of the hexagonal crystal structure, while the alloy is cubic.

CONCLUSIONS

As a result of this study of NbMo alloys of three different compositions we can say that the rigid band model gives fairly good agreement with the experimental data. The combination of these two particular transition metals does not appear to be unique. When Nb is alloyed with Ta, Zr and Y, a definite energy band structure persists, in spite of the disorder introduced as a result of alloying. More calculations must be done, however, to decide whether other models for alloys give a picture which is also in good agreement with the data.

Regardless of which theory we choose, we might expect to find trends as we go across a row or down a column in the periodic table. Yet our measurements do not show the Nb spectra shifting one way with the addition of Mo and the reverse way when alloying with Zr. Nor are shifts in opposite directions observed when we compare NbV with NbTa. This group of alloys presents some intriguing puzzles, and further study seems in order.

ACKNOWLEDGEMENTS

Dr. Lynch's readiness to offer suggestions or answer questions about anything and everything related to this study was greatly appreciated. Present and former members of the optical properties research group, both here and at Stoughton, gave help when it was needed. I would like to thank the people in metals development who prepared the alloy samples, and Harlan Baker, on whose expertise I relied for electropolishing them. Thanks are also due to those who assisted in putting this paper in its final form. Finally, family and friends, among whom I must particularly mention Rodney Black, kept me in good spirits when things got rough.

BIBLIOGRAPHY

1. F. Wooten, Optical Properties of Solids (Academic Press, New York, 1972).

2. J. N. Hodgson, Optical Absorption and Dispersion in Solids (Chapman and Hall, London, 1970).

3. D. W. Berreman, Appl. Opt. 6, 1519 (1967).

4. D. L. Greenaway and G. Harbeke, Optical Properties and Band Structure of Semiconductors (Pergamon Press, Oxford, 1968).

5. I. Petroff and C. R. Viswanathan, Phys. Rev. B4, 799 (1971).

6. L, F. Mattheiss, Phys. Rev. B1, 373 (1970).

7. D. W. Lynch, unpublished lecture notes. Physics 660B, Iowa State University (1973).

8. W. E. Pickett and P. B. Allen, Phys. Rev. B11, to be published.

9. J. H. Weaver, D. W. Lynch, and C. G. Olson, Phys. Rev. B7, 4311 (1973).

10. J. H. Weaver, D. W. Lynch, and C. G. Olson, Phys. Rev. B10, 501 (1974).

11. B. W. Veal and A. P. Paulikas, Phys. Rev. B10, 1280 (1974).

12. D. D. Koelling, F. M. Mueller, and B. W. Veal, Phys. Rev. B10, 1290 (1974)

13. S. Doniach, Phys. Rev. B2, 3898 (1970).

14. P. Abeles, "Optical Properties of Metals" in The Optical Properties of Solids, F. Abeles, ed. (North-Holland Publishing Company, Amsterdam, 1972).

15. I. Lindau and W. E. Spicer "Photoemission studies of alloys" in Charge Transfer / Electronic Structure of Alloys, L. H. Bennett and R. H. Willens, ed. (Metallurgical Society of AIME, New York, 1974).

16. P. O. Nilsson, Solid State Phys. 29, 139 (1974).

17. A. I. Golovashkin, I. E. Leksina, G. P. Motulevich, and A. A. Shubin, Zh. Eksp. Teor. Fiz. 56, 51 (1969) [Sov. Phys. - JETP 29, 27 (1969)]

18. L. W. Bos, Ph.D. Thesis, Iowa State University, Ames, Iowa, 1969 (unpublished).

19. L. W. Bos and D. W. Lynch, Phys. Rev. B2, 4784 (1970).

20. C. G. Olson and D. W. Lynch, Phys. Rev. B9, 3159 (1974).

21. R. P. Goodwin, Springer Tracts Mod. Phys. 50, 1 (1969).

22. E. L. Kreiger, D. J. Olechna, and D. S. Story, G. E. Research Lab Report No. 63-RL-3458G, 1963.

23. P. O. Nilsson and L. Munkby, Phys. Kond. Mat. 10, 290 (1969).

FIGURES

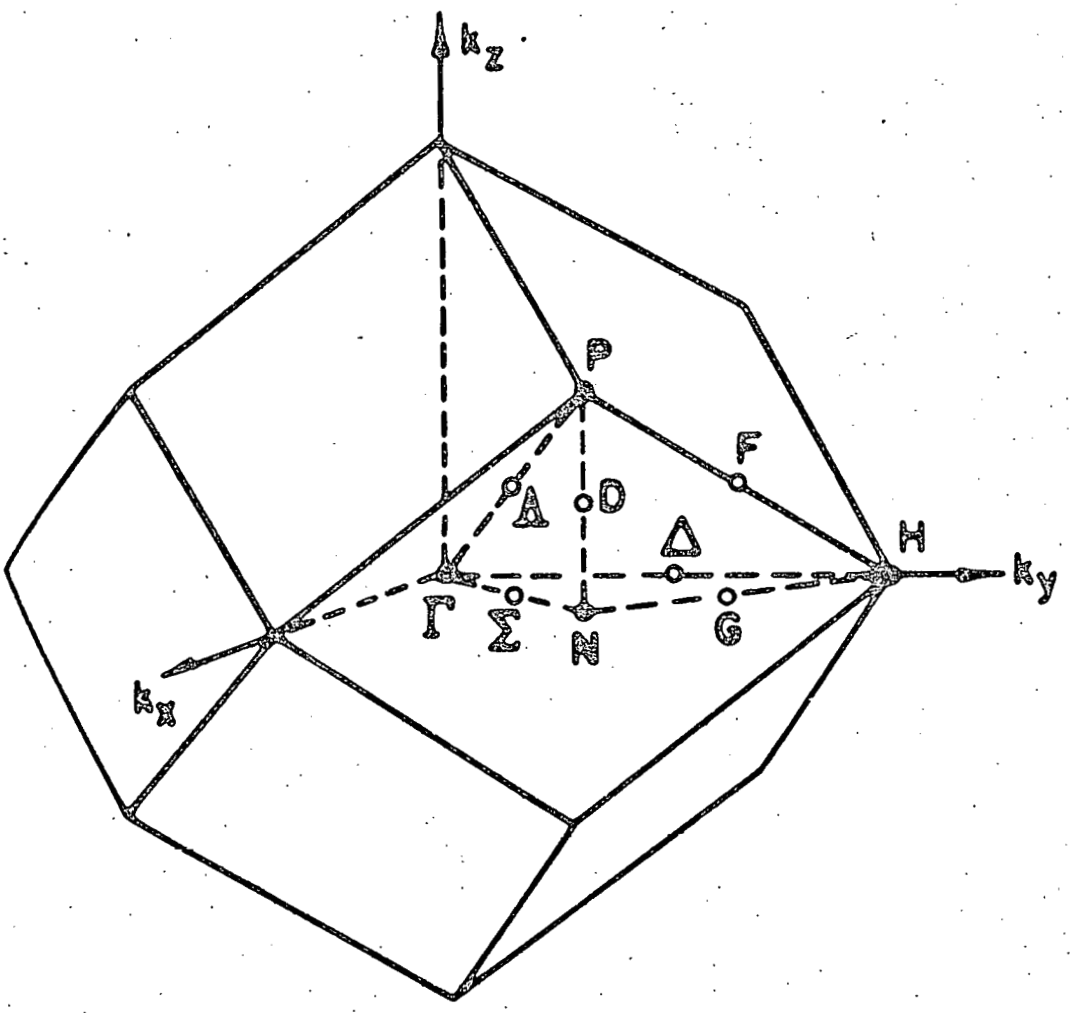

Figure 1. Points in reciprocal space for body centered
nic crystal structure.

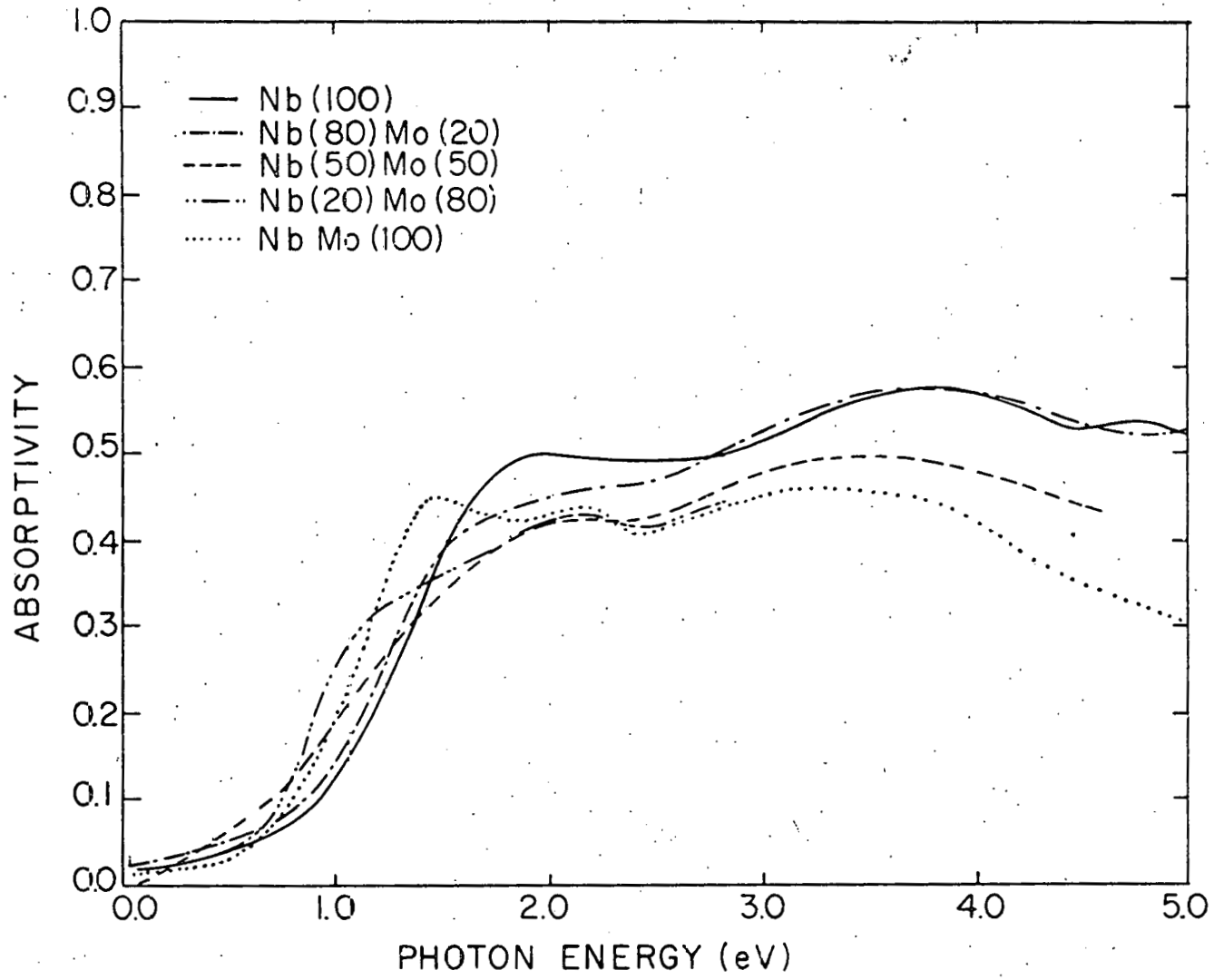

Figure 2. Low energy absorptivity of NbMo alloys of varying composition. The data were taken with the calorimeter.

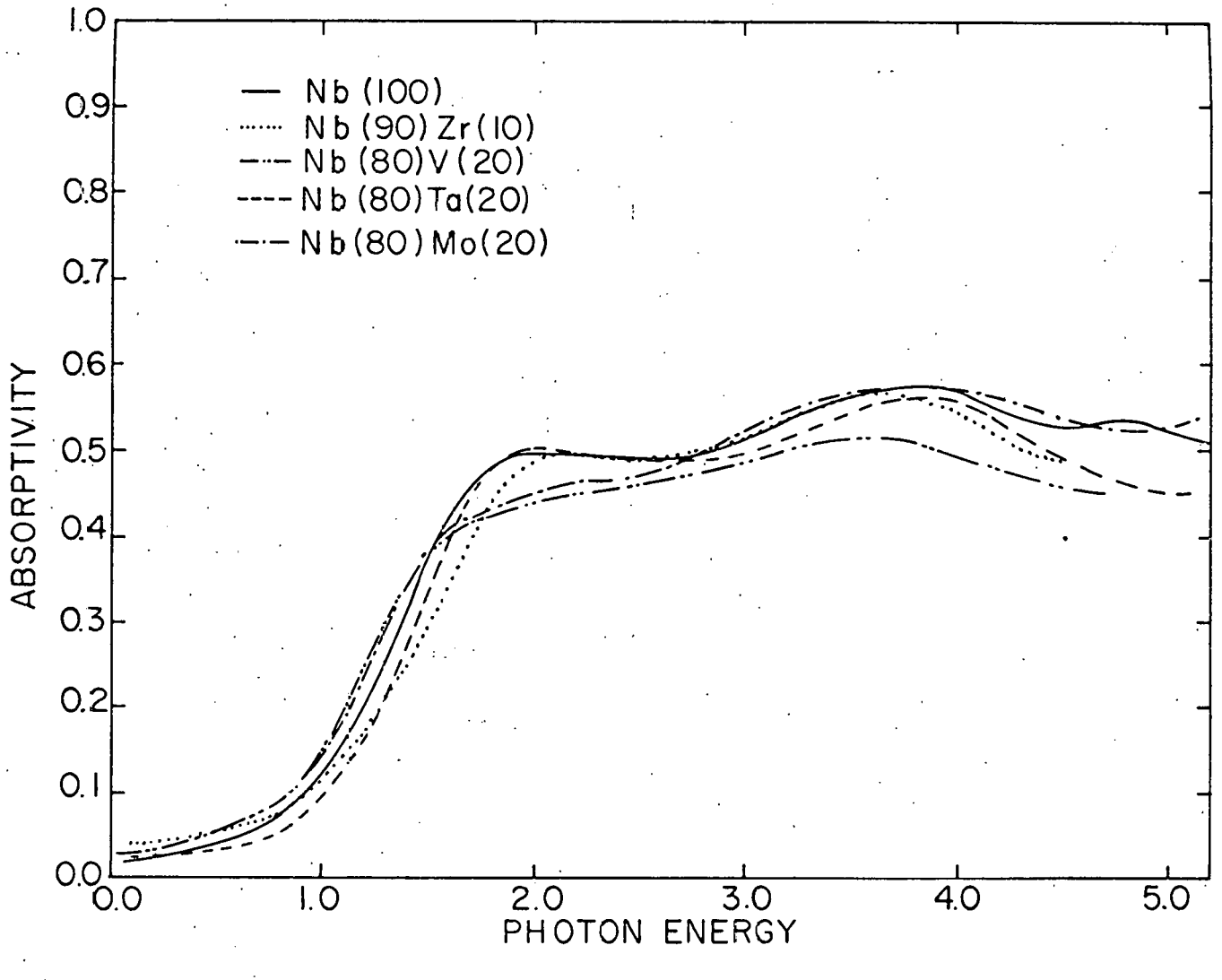

Figure 3. Low energy absorptivity of Nb alloyed with the transition metal adjacent to it in the periodic table. The data were taken with the calorimeter

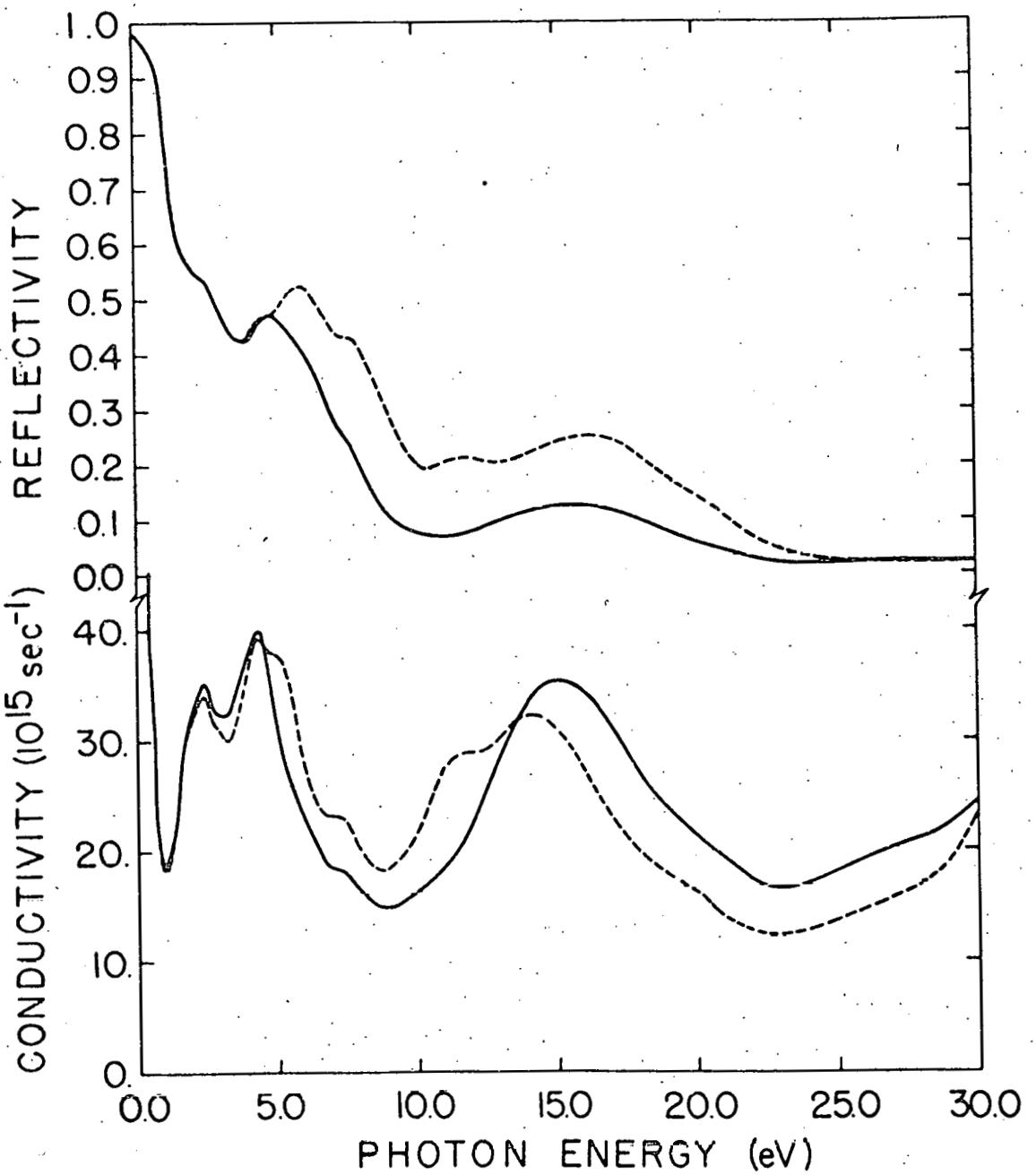

Figure 4. Reflectivity data and the conductivity resulting from Kramers-Kronig analysis of the data. Solid curves use data of Nb(80)Mo(20). Dashed curves use data for Nb above 4.2 eV.

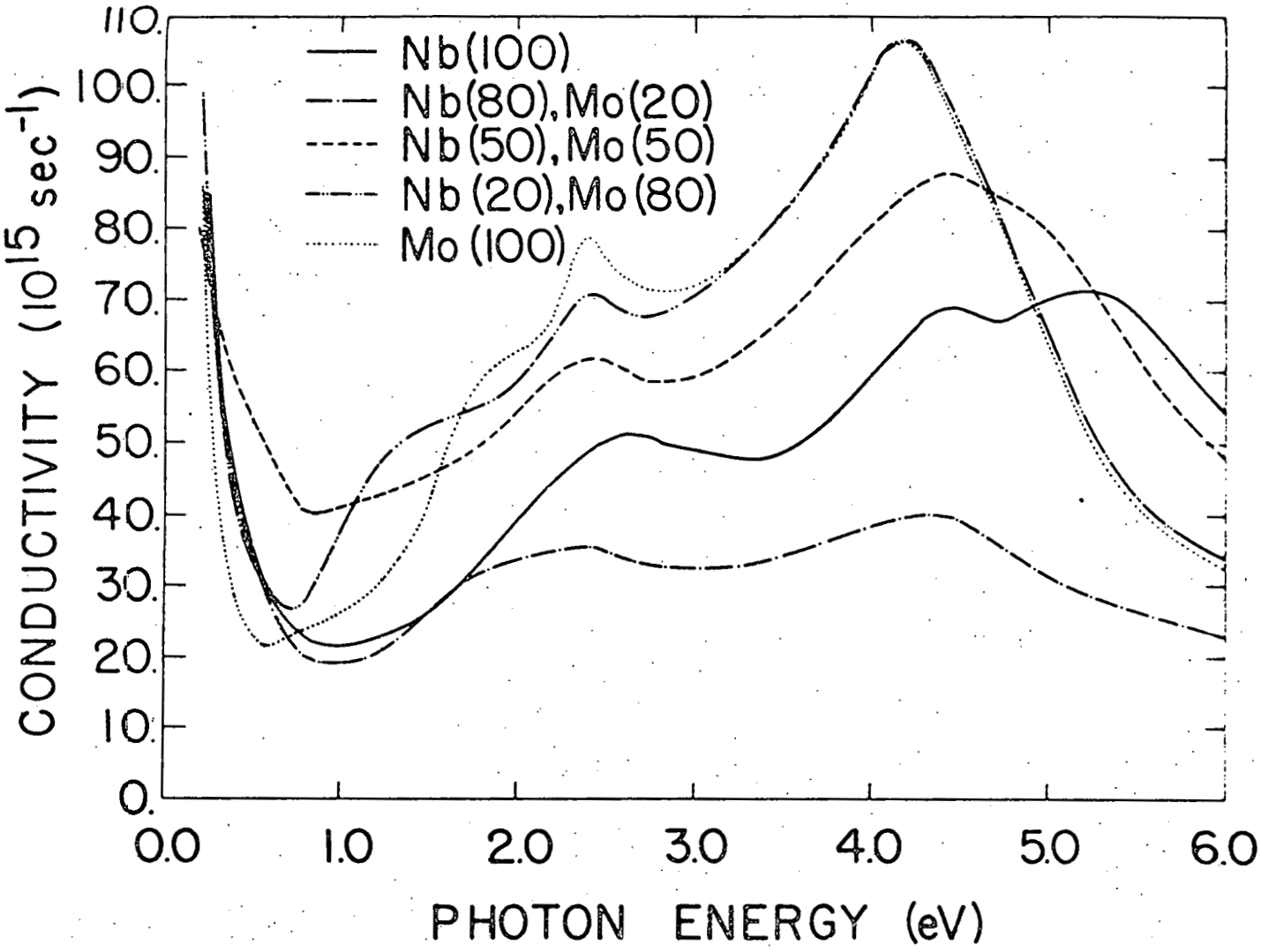

Figure 5. Conductivity for NbMo alloys of varying composition.

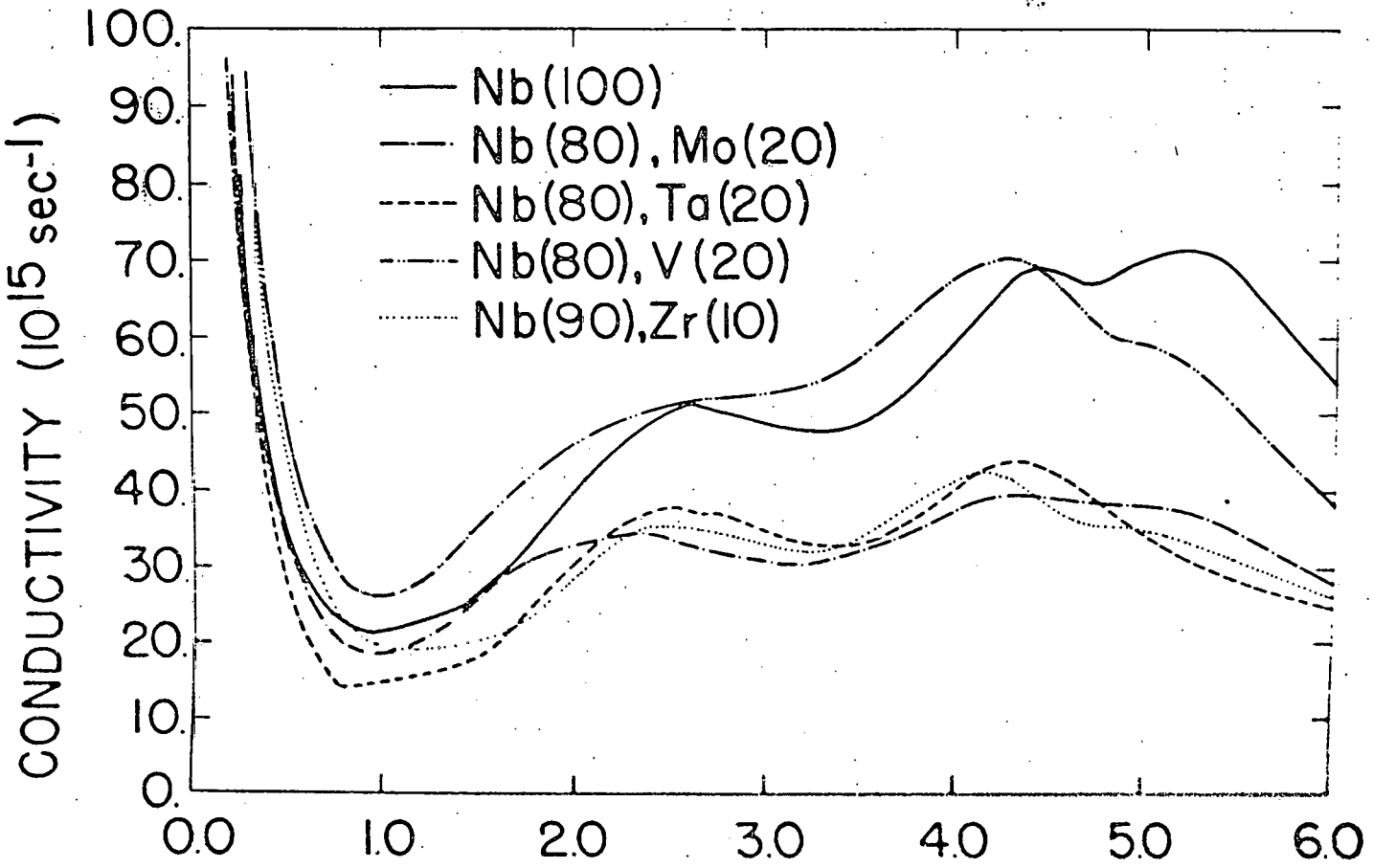

Figure 6. Conductivity for Nb alloyed with the transition metals adjacent to it in the periodic table.

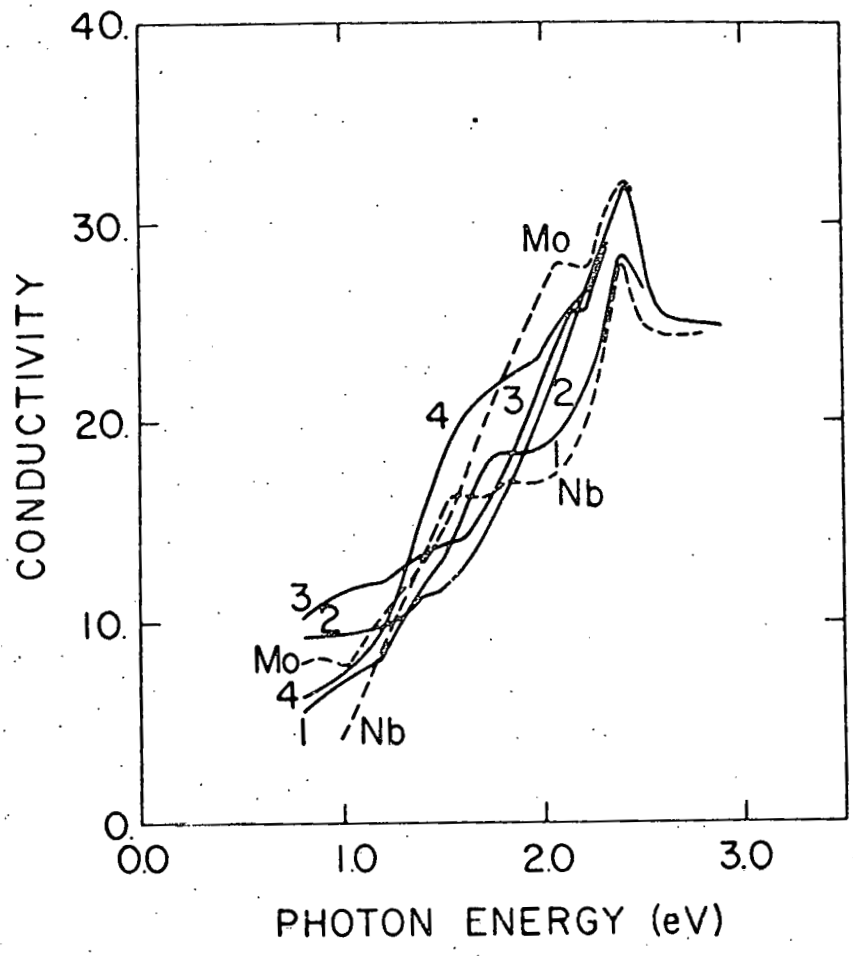

Figure 7. Calculated conductivity of the alloy series $Nb_{1-x}Mo_x$, x = 0.2, 0.4, 0.6, 0.8, denoted by 1, 2, 3, 4, respectively. From reference 8.

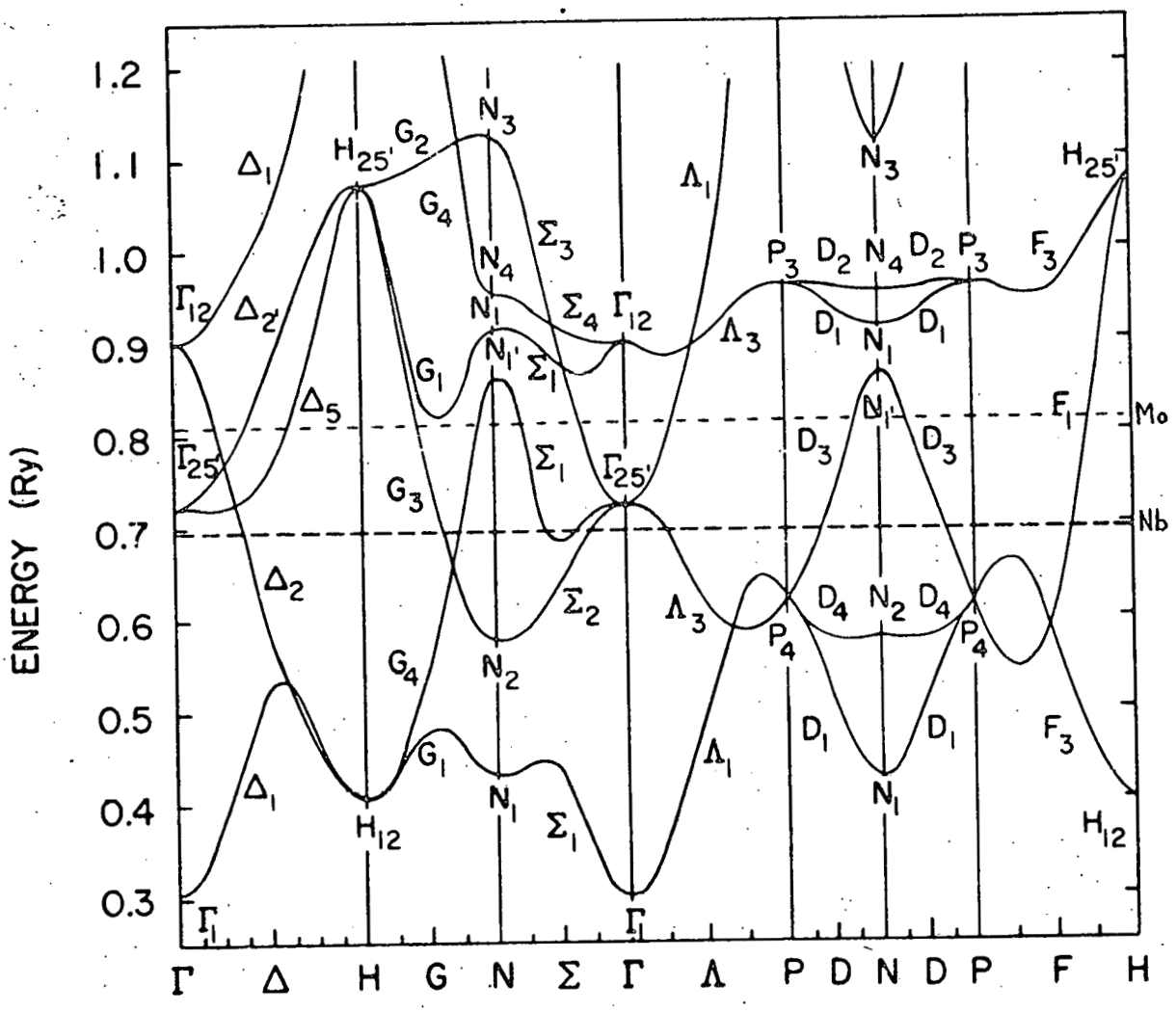

Figure 8. Energy band structure of Nb from L. F. Mattheiss, Phys. Rev. B1, 373 (1970). The Fermi level for Mo is indicated.